Manipulation and quantification of graphene oxide flake size: photoluminescence and cytotoxicity

Coleman, Brian R.; Knight, Timothy; Gies, Valerie; Jakubek, Zygmunt J.; Zou, Shan

Publisher's version / Version de l'éditeur:
https://doi.org/10.1021/acsami.7b08585
ACS Applied Materials and Interfaces, 9, 34, pp. 28911-28921, 2017-08-04

ACS APPLIED MATERIALS & INTERFACES

Research Article

www.acsami.org

Manipulation and Quantification of Graphene Oxide Flake Size: Photoluminescence and Cytotoxicity

Brian R. Coleman,[†] Timothy Knight,[†,‡] Valerie Gies,[†] Zygmunt J. Jakubek,[†] and Shan Zou*[,†,§]

[†]Measurement Science and Standards, National Research Council Canada, 100 Sussex Drive, Ottawa, Ontario K1A 0R6, Canada

[‡]Department of Physics, McMaster University, 1280 Main Street W., Hamilton, Ontario L8S 4L8, Canada

[§]Department of Chemistry, Carleton University, 1125 Colonel By Drive, Ottawa, Ontario K1S 5B6, Canada

Supporting Information

ABSTRACT: Single-layered graphene oxide (GO) has exhibited great promise in the areas of sensing, membrane filtration, supercapacitors, bioimaging, and therapeutic carriers because of its biocompatibility, large surface area, and electrochemical, photoluminescent, and optical properties. To elucidate how the physical dimensions of GO affect its intrinsic properties, we employed sonication to produce more than 130 different sizes of GO in aqueous dispersion and implemented new approaches to characterize various GO properties as a function of the average flake size. New protocols were developed to determine and compare the flake size of GO dispersions sonicated with energies up to 20 MJ/g by using dynamic light scattering and atomic force microscopy (AFM). The relationship between the average flake size and sonication energy per unit mass of GO was observed to follow a power law. AFM height measurements showed that the sonication of GO yielded monolayered flakes. Photoluminescence of GO was characterized as a function of the sonication energy (or the average flake size which is the monotonic function of the sonication energy), excitation wavelength, and pH of the dispersion. The strong dependence of the photoluminescence intensity on pH control and the variation of the photoluminescence intensity with different flake sizes were observed. An intense photoluminescence signal, likely related to the separation of the oxidative debris from the GO framework, was found at the highest sonication energies ($E \gtrsim 15$ MJ/g) or under extremely alkaline conditions (pH $\gtrsim 11$). The cytotoxicity of GO was studied with various flake sizes. Size- and concentration-dependent cytotoxicity was observed for cell lines NIH 3T3 and A549. The NIH 3T3 cell line also demonstrated time-dependent cytotoxicity.

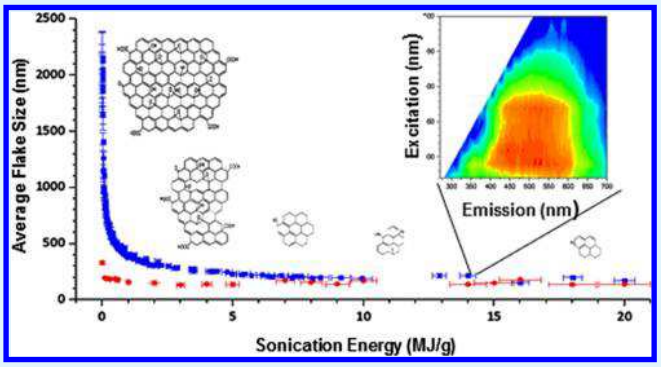

KEYWORDS: *sonication, dynamic light scattering, atomic force microscopy, pH dependent, cell viability*

INTRODUCTION

Graphene oxide (GO) has presented itself in recent years as one of the most exciting new materials of the future. In particular, GO is considered an important intermediate for the large-scale processing of graphene as it is highly soluble in aqueous media and can be readily reduced to graphene.[1−4] Two-dimensional (2D) morphology of single-layer GO has offered a great deal of possibilities for its use as an architectural template or a component of layer-by-layer assemblies with nanoparticles[5] and polymers.[6] GO presents interesting photoluminescent,[7,8] electrochemical,[9] structural,[10] and optical properties,[11] leading to its integration into sensors,[12−14] supercapacitors,[15,16] and drug-delivery vehicles.[17−19] To fine tune GO for various applications, more research is required to better understand the correlation between its flake size, morphology, and intrinsic properties. Large flakes with lateral dimensions in the millimeter range have been used in the fabrication of 2D[20] and three-dimensional (3D)[21] architectures because they demonstrate higher transparency and higher charge mobility in electrical devices compared with small GO flakes.[22] On the other hand, smaller flakes have proven useful for sensors[23] and biological applications.[24] Also, Shin et al. showed that small GO flakes produced by ball milling had higher electrorheological efficiency than the starting GO material.[25] Therefore, it is important to develop reliable flake size control methods and further explore the relationship between the GO flake size and intrinsic properties.

Several methods have been proposed to control the GO flake size. Sun et al. used density gradient ultracentrifugation (DGU) after chemical oxidation to separate different sizes of GO flakes.[26] Luo et al. used chemical exfoliation of crystalline graphite nanofibers to create a uniform population of GO nanosheets.[27] Others have used pH-assisted selective sedimentation[28] or chemical "scissors"[29] to control the GO flake size.

Received: June 14, 2017
Accepted: August 4, 2017
Published: August 4, 2017

DOI: 10.1021/acsami.7b08585
ACS Appl. Mater. Interfaces 2017, 9, 28911−28921

However, each of these methods suffers from one or more inherent flaws: DGU and pH-assisted selective sedimentation afford only low yields, graphite nanofibers are economically prohibitive, and chemical "scissors" utilize strong oxidizers.

Sonication has previously been used for graphite exfoliation and GO preparation.[30−33] It was demonstrated that large GO flakes were broken up by sonication in aqueous dispersions, hinting at an efficient and cost-effective method to control the flake size.[34] In another study, Luo et al. produced 30 nm GO nanosheets by sonicating graphite powder.[35] Ye and Feng sonicated GO powder for 2, 10, 30, and 60 min and observed completely exfoliated GO after 2 min, with further sonication resulting in a reduction of the average flake size.[36] Similar results were observed by Cai et al. who used atomic force microscopy (AFM) to measure flake sizes.[37] Recently, it was pointed out[36] that the sonication treatment for GO preparation lacks a systematic experimental control methodology. In the present work, we intend to further develop sonication of GO dispersions as a reliable flake size control method. The dispersions were processed with a tip ultrasonic processor that facilitated accurate control of the amount of transferred sonication energy. We explored the relationship between the total applied sonication energy and the average flake size of GO dispersions via systematic characterization by dynamic light scattering (DLS) and AFM.

Dispensing large amounts of sonication energy leads to flake fragmentation, but can also affect other GO properties. In addition to lateral dimensions, the thickness of GO flakes was measured by AFM to determine whether single or multiple layers had formed during sonication as several other methods of preparing GO had resulted in the presence of multilayered materials.[38,39]

In a recent study of GO photoluminescence, band intensities and peak excitation and emission wavelengths were observed to be dependent on pH values, which were attributed to the functional groups on the flake surface.[40] In an earlier work, sharp and structured molecular-like photoluminescence features were observed and assigned to originate from the coupling of carboxylic acid groups and carbon clusters in the graphene framework.[41] In the present work, GO photoluminescence intensity maps as a function of emission and excitation wavelengths were recorded at various sonication energies up to 20 MJ/g and pH values up to 11.5 to better understand the GO breakdown process and the relationship between the GO photoluminescence, average flake size, and pH value of the dispersion.

With increasing use of engineered nanomaterials, a thorough understanding of their interactions with biological systems is a key factor in the development of sustainable nanotechnologies.[42−44] GO and other graphene-based materials are potential candidates for drug-delivery and bioanalysis because of their ease of chemical modification and expected biocompatibility.[17−19] However, the issues of biocompatibility and toxicity of these materials remain unresolved as the research results obtained so far are somewhat conflicting. A popular method to study the cytotoxicity of nanomaterials is through the in vitro model using colorimetric assays such as MTT[45−49] and WST-8[45,49] (also known as CCK-8). The cytotoxicity of GO has been studied in the past on a variety of cell lines: A549 cells,[46,49] CRL 2522 cells,[45] HDF cells,[50] HeLa[47] cells, and HUVEC cells;[51] it was somewhat dependent on the dose, exposure time and flake size. Although various definitions of cytotoxicity have been in use, a common indicator of obvious toxicity is a final cell viability lower than 80%. Chang et al.[49] evaluated the cytotoxicity of three sizes of GO flakes on A549 cells using the WST-8 assay and observed that the cytotoxicity of GO is both dose- and size-dependent but not time-dependent. They concluded that GO hardly enters the cells and shows good biocompatibility. Wang et al.[50] studied the biocompatibility of in-house made GO, including its toxicity on human fibroblasts (HDF cells) and observed a dose-, time-, and size-dependent toxicity. Liao et al.[45] used two assays (MTT and WST-8) and observed GO to interfere with the MTT reagent, giving falsely high viabilities. This was not observed in other works that used the MTT assay.[46,47] Clearly, obvious differences between the results of various studies exist, and multiple issues such as the interference with the MTT assay, the overall toxicity of GO, and the time dependence of the cytotoxicity remain unresolved. These differences could result from varying properties of GO originating from different sources with different compositions and possible impurities and/or the different cell lines studied. As past GO toxicity studies have been inconclusive, more research is required. In this work, the toxicity of commercially available GO was studied with NIH 3T3 and A549 cells for three incubation periods and three flake sizes, using the WST-8 assay. Using the same source of commercially available GO potentially eliminates any variances in the composition or impurities of the GO samples and allows for the retrieval of reproducible data and reliable comparison of results.

EXPERIMENTAL SECTION

Materials. For sonication and photoluminescence studies, raw materials of GO were purchased from Graphenea Inc. (Cambridge, MA, USA) as 0.5 mg/mL dispersion in water and from Angstron Materials (Dayton, OH, USA) as 1.0 wt % dispersion. For the cytotoxicity studies, 4 mg/mL dispersion of GO in water was purchased from Graphenea Inc. and diluted to 2 mg/mL, with water as the stock solution for further dilutions. Milli-Q water (Millipore, Billerica, MA, USA) deionized to 18.2 MΩ cm was used in all experiments.

Sonication. The GO dispersions were diluted to a target concentration of 0.21 mg/mL by adding 10 mL of water to 7.5 mL of the as-received 0.5 mg/mL Graphenea dispersion or 17.125 mL of water to 0.375 mL of the as-received Angstron dispersion. The diluted dispersions were mixed by inversion and sonicated with various energies using a 130 W ultrasonic processor (Cole-Parmer, Vernon Hills, IL, USA) equipped with a 6 mm probe. Sonication was performed in a cold−water bath (∼4 °C) and in intervals (15 min sonication/1 min cooling) to prevent excessive heating of the dispersions. The average sonication power, as indicated by the processor display, was 10 W for all samples.

AFM Imaging. AFM height/topography images were recorded using both NanoWizard II BioAFM (JPK Instruments, Berlin, Germany) mounted on an Olympus IX81 inverted microscope and MultiMode NanoScope V with PeakForce QNM mode (Bruker Nano Surfaces Division, Santa Barbara, CA, USA). XSC-11 tips (Cantilever D, MikroMasch, CA, USA) with a typical spring constant of ∼42 N/m and a resonance frequency of ∼350 kHz were used for images captured with a JPK atomic force microscope. Additionally, ScanAsyst-Air probes (Bruker AFM Probes, Camarillo, CA, USA) with a typical spring constant of 0.4 N/m and a resonance frequency of 50−90 kHz were used. The peak force was always kept at the lowest stable imaging level of 200−500 pN.

Samples for AFM were made by spin-coating diluted GO dispersions (40 μL, 0.05 mg/mL) onto freshly cleaved 1 cm by 1 cm squares of mica substrate at 3000 rpm for 45 s. For each condition, three samples were prepared, and for each sample, three to five images were recorded at three to five different locations on the mica surface, for a total of nine to fifteen images per sample. The scan ranges of the images were 10 μm by 10 μm or 20 μm by 20 μm.

DOI: 10.1021/acsami.7b08585
ACS Appl. Mater. Interfaces 2017, 9, 28911−28921

Size and Height Measurements. AFM image processing and analysis were performed with Gwyddion open source software with well-documented operation and functions. Details of the determination of the flake size can be found in the Supporting Information. Briefly, to facilitate automated analysis, images were flattened in Gwyddion to correct for drifts during scanning. The threshold was set at half of an average flake gray value, which corresponds to height, and the flakes were selected by masking all pixels above the threshold. Finally, the maximum Feret's diameter (the maximum distance between two parallel lines tangent to the flake circumference) or the flake area was measured for each masked flake. The flake areas were next converted to equivalent circle (circle with the same area as that of a flake) diameters using the $d = 2\sqrt{\text{area}/\pi}$ formula. The Feret's diameter was further used as the flake size descriptor for comparison with DLS results.

Only isolated flakes were measured; images were typically recorded with a large scan area (20 μm by 20 μm) to minimize the bias (see Supporting Information for details). Features with an area smaller than 4 pixels were excluded (also see Supporting Information for details). The workflow of the AFM analysis is illustrated in Figure S1 (see also Table S1 for size distributions).

Isolated flakes were chosen for height measurements. To minimize the analyst bias in the measurement and to average noise effects and variability of the GO flake flatness, the flake height was measured by taking three profiles along the slow AFM scan direction for each flake: one at the top, one in the middle, and one at the bottom of the flake (Figure S2A). Variation of the vertical displacement value in the flake and background areas resulted from variation of the flake thickness and residual background curvature and roughness, respectively, as well as from noise and other instrumental and ambient effects. The three profiles measured along these lines are shown in Figure S2B–D. The minimum and maximum height values were recorded for each trace, and the average value was calculated to represent the flake thickness (the background is assumed to be 0).

DLS Measurements. GO dispersions were diluted for DLS measurements to a concentration of 0.002 mg/mL using Milli-Q water. The measurements were performed using a Zetasizer Nano ZS (red) particle size analyzer (Malvern Instruments, Worcestershire, UK). For each sample, three measurements consisting of ten 10 s-long runs were taken. The measurements were conducted at 25 °C with 120 s-long initial equilibration time.

DLS measurements yielded for each sample an intensity-weighted arithmetic-average equivalent sphere hydrodynamic diameter, which was used as the flake size DLS descriptor. The equivalent sphere hydrodynamic diameter is the diameter of a sphere that diffuses through the dispersion via Brownian motion at the same rate as the measured particles.[52] The average sphere diameter was determined for the dominant population in those cases when multimodal distribution of flake sizes was recovered from the analysis.

Photoluminescence of GO. Photoluminescence spectra of GO samples were recorded with a Fluorolog Tau-3 spectrofluorometer (Horiba Jobin Yvon, Edison, NJ, USA) with face excitation using thin quartz cuvettes oriented at 45° with respect to the excitation beam. The spectra were recorded with the excitation in the 250–510 nm range in 20 nm steps and emission detection starting 10 nm to the red of the excitation wavelength and continuing up to 700 nm in 3 nm steps. To minimize bleaching, the spectra acquisition started with the excitation at the longest wavelength in the excitation range and advanced to the blue. The samples were mixed inside the cuvette between scans to reduce the potential effects of bleaching on the spectra.

Photoluminescence spectra were edited by removing water Raman and second-order Rayleigh scattering peaks, allowing these regions to be smoothed by the OriginPro 8 software. An elevated background was observed for λ_{ex} = 250, 270, and 290 nm; as the background signal was rather noisy for these excitation wavelengths, a scaled background correction procedure with multipliers 0.05, 0.5, and 0.9, respectively, determined from averaged background scans rather than direct background subtraction, was used.

Dispersion Stability Measurements. Stability measurements of GO dispersions under highly basic conditions were performed with a Turbiscan LAB stability analyzer (Formulaction SA, L'Union, France) at 37.5 °C with the initial equilibration time of 10 min. Transmission and backscattering profiles were acquired with 40 μm steps along the cell height every hour over a span of 24 h.

Cytotoxicity Study. Graphenea GO dispersions were prepared by probe sonicating 10 mL of 2 mg/mL GO in sterile water (autoclaved at 121 °C for 30 min) for a predetermined amount of time to create samples with three approximate average flake sizes: 150, 250, and 850 nm (by DLS). Cell media [Dulbecco's modified Eagle's medium (DMEM) and F-12K], fetal bovine serum (FBS), and penicillin streptomycin were purchased from Gibco (Thermo Fisher Scientific Inc., Burlington, ON, Canada). NIH 3T3 (immortal, murine embryo fibroblast) cells were cultured in DMEM and A549 (immortal, human lung epithelium) cells were cultured in F-12K, both supplemented with 10% heat-inactivated FBS and 1× penicillin streptomycin in an incubator at 37 °C with 5% CO_2 and a high relative humidity. GO toxicity studies were performed in 96-well, flat-bottom plates (BD Falcon, purchased from VWR International LLC., Mississauga, ON, Canada), and the cells were seeded to a density of (1.5–2.5) × 10^4 cells/well, depending on the cell line. The cells were exposed to various concentrations of GO (5, 10, 20, 30, 50, 75, 100, and 200 μg/mL) for 24, 48, and 96 h. Following the exposure period, 10 μL of the WST-8 reagent (Cedarlane Laboratories Limited, Burlington, Canada) was added to all wells, and the well plate was incubated for 4 h. The optical densities of the WST-8-treated samples were measured at 450 nm on a FLUOstar Omega microplate reader (BMG Labtech, Ortenberg, Germany).

RESULTS AND DISCUSSION

Control of GO Flake Size and Size Measurements. Sonication treatments have been commonly used in graphite exfoliation and GO preparation.[30−33] It was previously pointed out that the sonication treatment for GO preparation lacks systematic experimental control methodology.[36] In the present work, we explore the relationship between the total sonication energy and the average flake size of GO dispersions. Graphenea and Angstron GO samples were sonicated with various amounts of energy per unit mass of GO present in dispersions up to 20 MJ/g. The flake size of multiple sonicated dispersions was measured by AFM (Figure S1, Table S1) and DLS (Figure 1, Tables S2 and S3). Although AFM can provide a rather accurate description of both lateral and vertical dimensions of a single flake as well as ensemble size distributions, the method is tedious and time-consuming as a large number of images must be recorded and analyzed, which rarely is the case. DLS, in comparison, facilitates a much faster and less expensive assessment of the average flake size and size distribution, although only equivalent size, the equivalent sphere hydrodynamic diameter, is determined. Although both methods have their limitations, DLS appears to be more advantageous compared with AFM for fast GO flake size assessment, especially when a large number of samples are to be analyzed and a relative size description, as opposed to an absolute size description, is sufficient. It should be pointed out that even though the measurands (size and size distribution) are defined somewhat differently by the two methods and comparison of DLS and AFM results is not straightforward, both methods can effectively be used to monitor the size variation as a function of the sonication energy.[55,56] Even though both DLS and AFM have previously been used to measure the GO flake size, no systematic evaluation of the relationships between both size descriptors and the corresponding applied sonication energy has been conducted.[29]

DOI: 10.1021/acsami.7b08585
ACS Appl. Mater. Interfaces 2017, 9, 28911−28921

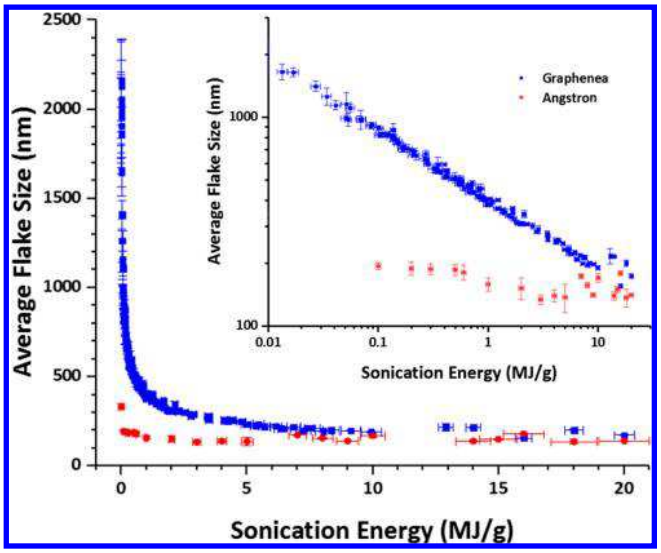

Figure 1. Average DLS-measured flake size as a function of sonication energy for Graphenea (blue, 136 samples) and Angstron (red, 20 samples) GO dispersions. The inset displays a log−log plot of the size as a function of the sonication energy for both GO materials, illustrating that the power law governs the fragmentation of GO flakes. The vertical error bars shown for selected points correspond to plus and minus 1 standard deviation of three repeat DLS measurements. The horizontal error bars are plus and minus 1 standard error of the sonication energy per unit mass of GO. All samples had a polydispersity index (PDI) between 0.2 and 0.5 and a count rate optimized to the signal-to-noise range.

The intensity-weighted average hydrodynamic diameter determined by DLS was compared with the number-weighted average Feret's diameter measured by AFM, and both size descriptors were analyzed as a function of the sonication energy (see Table S1). Here, the focus was on the relative size variation with the sonication energy, the comparison between an intensity weighted size descriptor by DLS and a number weighted one by AFM, was deemed acceptable. It was observed that the average GO flake size could be reliably controlled through sonication in a wide range of sizes. In the 0−20 MJ/g range of sonication energies, the average hydrodynamic diameter of the Graphenea GO flakes varied from ∼2000 down to ∼170 nm and for the Angstron GO flakes from ∼330 to ∼140 nm. Figure 2 shows the size measurement results of AFM (average Feret's diameter) and DLS (hydrodynamic diameter) for Graphenea and Angstron GO materials in a log−log plot as a function of the applied sonication energy. It should be noted that the as-received flake sizes of the two materials are different, with the Angstron and Graphenea GO flake average DLS hydrodynamic diameters of ∼330 and ∼2000 nm, respectively. Both AFM and DLS flake sizes, when plotted as a function of the sonication energy, show a rather dramatic decrease with increasing energy up to ∼1.5−2 MJ/g to slowly level at higher energies. However, in the log−log plot (see Figures 1 inset, 2A, and S3), a linear relationship is apparent, which indicates that the flake fragmentation by sonication is governed by a power law in the range of sonication energies studied in this work. The DLS power function fits yielded the following size-energy relationships: $\overline{d}_h = 408.17 \times 10^{-0.324}$ for Graphenea GO ($R^2 = 0.9901$) and $\overline{d}_h = 168.95 \times 10^{-0.053}$ for Angstron GO ($R^2 = 0.4652$), where E is the sonication energy in MJ/g and $\overline{d}_h$ is the hydrodynamic diameter in nm. Power function fits for the AFM measurements of Graphenea GO and Angstron GO are $\overline{d}_F = 558.85 \times 10^{-0.536}$ ($R^2 = 0.8955$) and $\overline{d}_F = 223.33 \times 10^{-0.149}$ ($R^2 = 0.6545$), respectively, where E is the sonication energy in kJ/g and $\overline{d}_F$ is the average Feret's diameter in nm. The flake size analyses yielded number-weighted (AFM) and intensity-weighted (DLS) flake size distributions. The DLS determined size distributions appear systematically narrower (PDI ranging from 0.2 to 0.5) compared with the AFM determined ones (Figure 2B−E), which may indicate some aggregation of substrate-deposited flakes, but also reflect a method-specific effect.

The observed power law variation of the flake size with the sonication energy is consistent with the recent work by Gonçalves et al.,[53] who suggested a two-step breakdown pathway of GO flakes via sonication. Initially the GO flakes are broken in regions with a large proportion of sp^3 bonds (C−OH and O−C−O) as these areas do not benefit from the strength inherent to sp^2 bonds. Breakage in these areas causes a rapid decrease in the size of the flakes as the large flakes are broken into smaller pieces. The second stage involves the removal of functional groups (COOH and C═O) from the periphery of the material, leaving behind sp^2 bonds and a more hydrophobic material. Gonçalves et al. hypothesized that this is the result of sonication causing the degradation of water molecules into high-energy hydroxyl radicals, which then act to reduce the carboxyl and carbonyl groups (dubbed hot spot atomic reduction).[53]

Several methods of GO production have been observed to yield multilayered flakes. As multilayered GO flakes have different properties than single-layered ones,[54,57] it is important to evaluate how sonication affects the flake thickness. Using AFM, the flake thickness was measured for both unsonicated and sonicated GO, the results of which can be found in Figure S2.

The average flake height for both the samples is approximately the same at ∼1.0 nm, a typical value for GO on a mica substrate.[48] Figure S2E,F shows the histograms for the flake heights collected for unsonicated and 1.3 MJ/g sonicated Graphenea GO. We concluded that the average flake thickness is not affected by sonication. Therefore, sonication preserves the monolayer morphology of GO flakes.

Photoluminescence of GO. GO dispersions are known to luminesce when excited with specific wavelengths of light. The photoluminescence has been attributed to two separate mechanisms: electron−hole recombination across the band gap defined by the size of the sp^2 clusters found within the carbon framework[40] and the presence of functional groups on the GO sheets (C−O, C═O, and O═C−OH).[58] In this work, photoluminescence has been probed as a function of the average flake size and pH value of a dispersion by acquiring 2D photoluminescence spectra with the excitation wavelengths varying in the 240−500 nm range and emission wavelengths in the 260−700 nm range. The flake size was controlled by tuning the sonication energies, which resulted in the average flake sizes of the dominant fraction (with sonication energy shown in parentheses) equal to 458 nm (0.6 MJ/g), 243 nm (4 MJ/g), 161 nm (12 MJ/g), 171 nm (16 MJ/g), and 194 nm (20 MJ/g). For each of the sonicated dispersions, pH was adjusted to approximately 2, 4.5, 7.5, 10, and 11.5 by the addition of HCl or NaOH (see Figure 3). Graphenea GO dispersions were selected for photoluminescence studies as this material displayed fewer defects under AFM and was expected to give a better representation of the GO framework (Figure S4).

DOI: 10.1021/acsami.7b08585
ACS Appl. Mater. Interfaces 2017, 9, 28911−28921

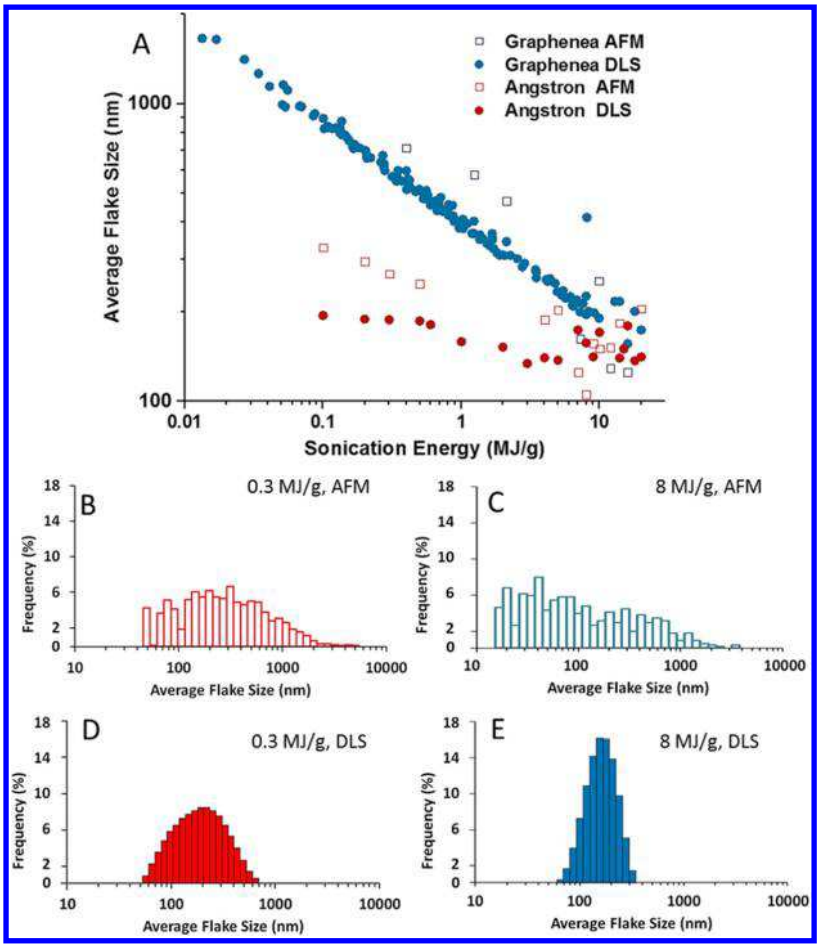

Figure 2. (A) log–log plot of average flake sizes of Angstron and Graphenea GO as a function of sonication energy measured by AFM and DLS. Representative histogram of the average size determined by AFM for (B) Angstron GO sonicated with 0.3 MJ/g and (C) Graphenea GO sonicated with 8 MJ/g. (D,E) Corresponding size histograms measured on the same sample of (B) and (C) by DLS, respectively.

A very clear trend in the intensity is present as the pH increases from 2 to 11.5. The intensity of the band gap photoluminescence in the $\lambda_{ex} \approx 300-400$ nm and $\lambda_{em} \approx 400-600$ nm range becomes steadily weaker with increasing pH. Around or slightly above pH 4.5, the intensity of this region drops substantially, coinciding with the deprotonation of the carboxylic acid groups found on the GO framework. At pH 10, the band gap photoluminescence signal disappears completely, perhaps coinciding with the deprotonation of the phenol groups (pH ≈ 8).[59] Despite the substantial loss of intensity with increasing pH, the band gap photoluminescence appears to be present for all pH values across all sonication energies, with the emission maximum apparently shifting to the blue. The shift is clearly related to the emergence of the narrow band at $\lambda_{ex} \approx 290$ nm at high pH. Figure 4 depicts this trend for the 12 MJ/g sonicated samples showing the 370 nm excited normalized spectra for all investigated pH values. The variation of the band gap photoluminescence intensity may be a result of size change of the sp^2 carbon clusters inherent to the material because of modification of the electronic structure mediated by the protonation status of surface groups as well as fragmentation of flakes and/or change of density of the framework defects. A relatively small variation of the luminescence intensity with increasing sonication energy and a strong decrease with increasing pH would appear to indicate that the protonation status of the surface groups plays the dominant role. However, because of a rather weak photoluminescence signal and large intensity fluctuations, extraction of more details on photoluminescence trends was not feasible.

At a high pH (11.5), a strong and relatively narrow photoluminescence band at $\lambda_{ex} \approx 290$ nm and $\lambda_{em} \approx 350-450$ nm can be observed. Previous work by Rourke et al. suggests that this signal may arise from a highly oxidized component of GO, the oxidative debris (OxD), which is attached to the main GO framework and is able to separate under basic conditions.[60−62] To examine this suggestion, highly alkaline GO dispersions (pH ≈ 14) sonicated with 0.6, 4, and 20 MJ/g energy were created. All three samples were phase-separated (Figure 5A) into a black flocculate (the base washed GO or bwGO) and a "clear" solution (OxD) layer.

Photoluminescence maps (Figure 5B–D) for the OxD layer solution showed intense peaks centered at $\lambda_{ex} \approx 290$ nm and $\lambda_{em} \approx 350-450$ nm, indicating that the OxD may be responsible for this intense photoluminescence signal. As the highly alkaline environment has deprotonated the functional groups on the GO surface, this likely creates enough electrostatic repulsion between the heavily oxidized OxD and the underlying GO framework to cause a separation. Once free, OxD ceases to act as a surfactant, causing the more hydrophobic bwGO to flocculate. Stability measurements conducted with a Turbiscan LAB analyzer showed that the GO dispersions remained stable with pH increasing up to ~12.3, at which point the onset of aggregation was observed (Figure S5).

DOI: 10.1021/acsami.7b08585
ACS Appl. Mater. Interfaces 2017, 9, 28911−28921

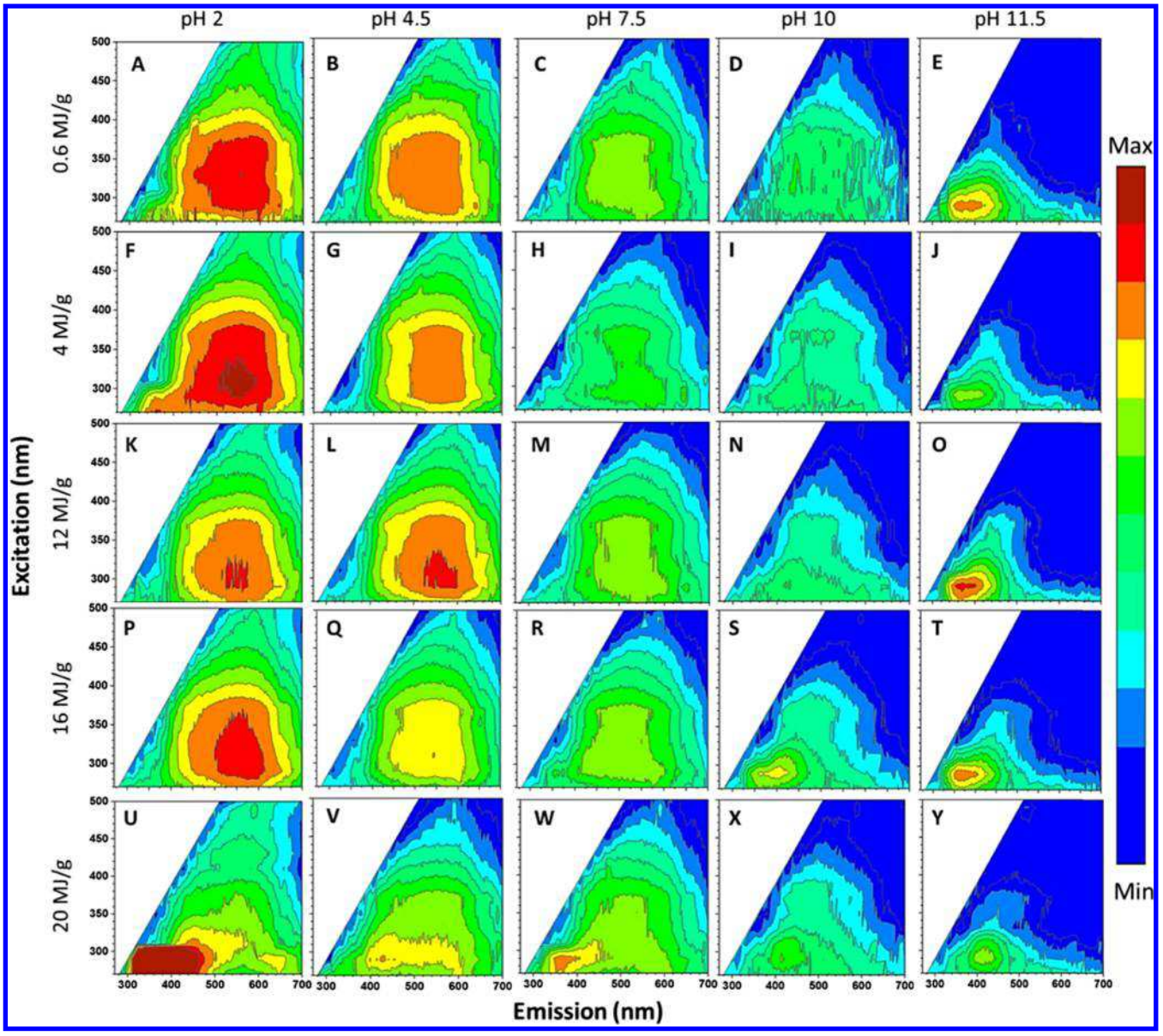

Figure 3. (A–Y) A set of 2D photoluminescence maps for Graphenea GO dispersions sonicated with varying amount of energies up to 20 MJ/g and pH ranging from 2 to 11.5. The spectra were corrected for variations in the excitation light intensity, but not for the variation of detection efficiency with wavelength. As a consequence, the apparent luminescence intensity in the emission long wavelength range is somewhat suppressed compared with the fully corrected signal. All spectra were recorded with the same instrument settings and are displayed on the same intensity scale with arbitrary units. The intensity of all plots is scaled logarithmically. Excitation wavelengths ranged from 270 to 500 nm. Emission wavelengths ranged for each scan from 20 nm to the red of the excitation wavelength and continuing up to 700 nm.

For the dispersions sonicated with 20 MJ/g of energy (Figure 3U–W), an intense band centered at $\lambda_{ex} \approx 290$ nm and $\lambda_{em} \approx 350–450$ nm can be observed across the entire range of pH values. In addition, a similar band also appeared for the dispersion sonicated with 16 MJ/g, but only for the two highest pH values. The intense bands observed for the dispersions sonicated with the highest energy and those for dispersions with the highest pH value all appear to share the same excitation wavelength and cover the same emission wavelength range. Therefore, we believe that the detachment of the OxD may be induced by either highly basic conditions in the dispersion or excessive sonication or a combination of both. Occasionally, a strong luminescence signal at the excitation and emission wavelengths corresponding to those of the OxD-assigned band was observed for low-sonication-energy samples (Figure 6). This would suggest that other factors may exist, inducing OxD detachment in dispersions.

Size Dependence and Cell Cytotoxicity. In this work, we have investigated the cytotoxicity of GO as a function of the flake size, concentration, and treatment time. GO flakes are expected to show enhanced biocompatibility compared with other graphene-based materials because of a large number of hydrophilic groups on their edge and basal plane. NIH 3T3 mouse embryonic fibroblast cells and a human lung carcinoma epithelial cell line A549 were evaluated after GO exposure. Figure 7 demonstrates the viability of NIH 3T3 and A549 cells in the presence of GO flakes of three different sizes after 24, 48, and 96 h of incubation, as measured by the WST-8 assay. The average size of the GO flakes, as determined by DLS and AFM (Table S4), respectively, was (A) (147 ± 4) and (159 ± 7) nm,

DOI: 10.1021/acsami.7b08585
ACS Appl. Mater. Interfaces 2017, 9, 28911–28921

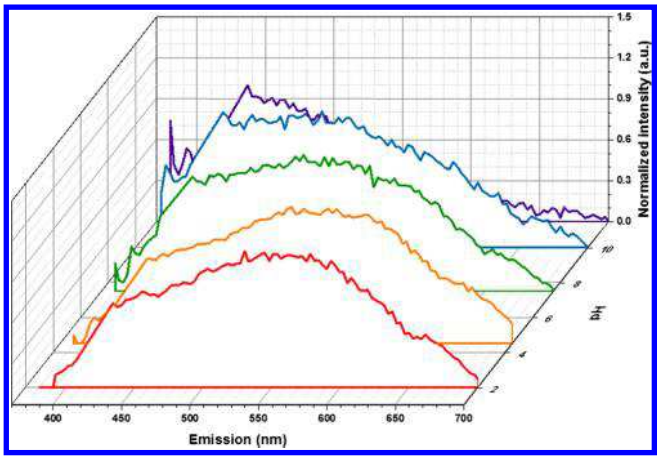

Figure 4. Photoluminescence spectra excited at 370 nm for the 12 MJ/g sonicated samples for various pH values, as indicated in the plot.

(B) (220 ± 1) and (239 ± 12) nm, and (C) (896 ± 9) and (867 ± 29) nm. To calculate the viability of the cells after GO treatments at n μg/mL, the following equation was used

$$\text{Viability} = \frac{OD_s - OD_{sb}}{OD_c - OD_{cb}} \quad (1)$$

Where OD_s, OD_{sb}, OD_c, and OD_{cb} are the optical densities of a sample, sample blank, control, and control blank, respectively. The flake size effect on GO cytotoxicity was observed for both cell lines, with smaller flakes showing greater toxicity. The effect is most obvious for the 24 h incubation period as the impact of evaporation and the variability of the original cell seeding density is the least significant. However, it is observed for longer incubation periods as well. After 24 h exposure to 200 μg/mL of GO with the largest flake size, up to 20% of the cells remained viable, whereas no viable cells were observed when treated with the smallest flake size GO. The size effect is more prevalent for the NIH 3T3 line, perhaps because of the higher overall toxicity and therefore an enhanced response due to the flake size variation. The impact of the flake size on the cytotoxicity of GO was previously studied by other groups, which used formazan-based assays.[45,46,49] In those cases, a size-dependent toxicity was observed; smaller sizes of GO resulted in lower cell viability, which agrees well with the findings of this work. It is expected that small flakes are more likely to become internalized by the cells and therefore show increased cytotoxicity, though more research should be performed to demonstrate the route of toxicity.

Obvious evidence of GO toxicity was observed for the NIH 3T3 cell line at concentrations exceeding 20 μg/mL, regardless of the flake size. The cytotoxicity was also determined to be time-dependent as longer exposure time resulted in lower viability. Similar results indicating time-dependent toxicity with GO concentrations exceeding 20−25 μg/mL have previously been published.[45] It was noted that aggregates were observed for GO concentrations equal to or above 75 μg/mL dispersions for all sizes studied. Though the aggregates may reduce the apparent toxicity of the GO sample, 75 μg/mL and higher concentrations of GO are well above concentrations that resulted in obvious toxicity. Furthermore, aggregation occurred for all sizes of GO and does not impact the size-based toxicity conclusions.

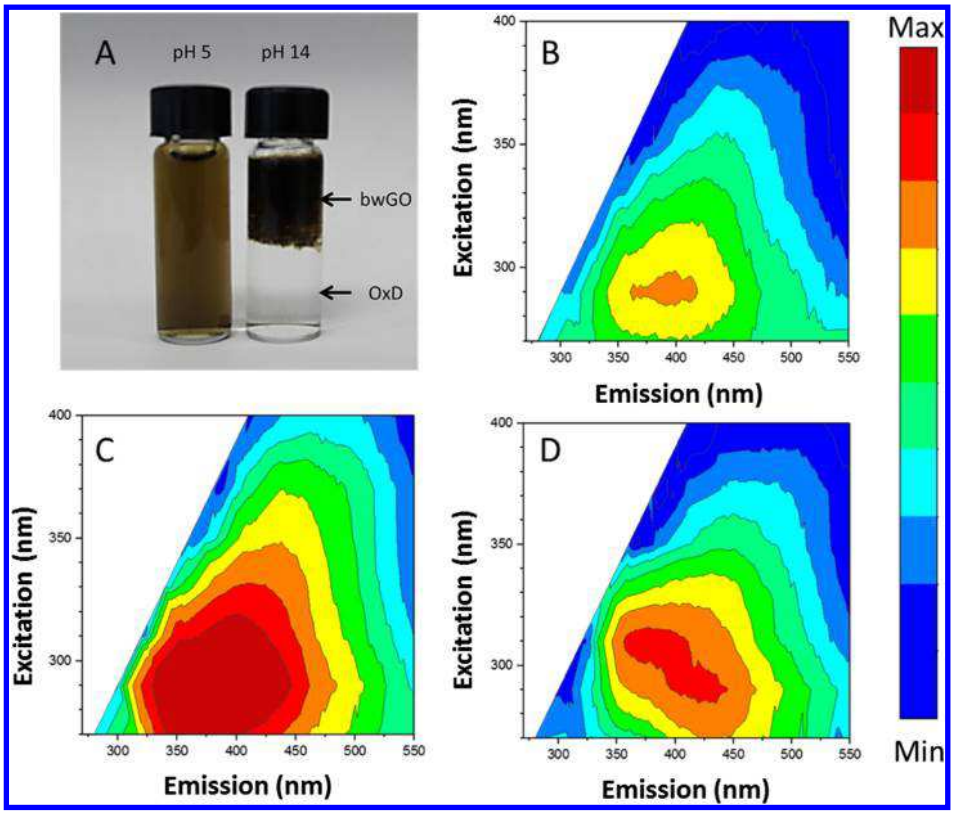

Figure 5. (A) Photograph of GO aqueous dispersions at pH 5 and 14. Photoluminescence maps for the "clear" OxD bottom layer for samples sonicated with (B) 0.6, (C) 4, and (D) 20 MJ/g energy. The intensity values of all plots are on the same logarithmic scale.

DOI: 10.1021/acsami.7b08585
ACS Appl. Mater. Interfaces 2017, 9, 28911−28921

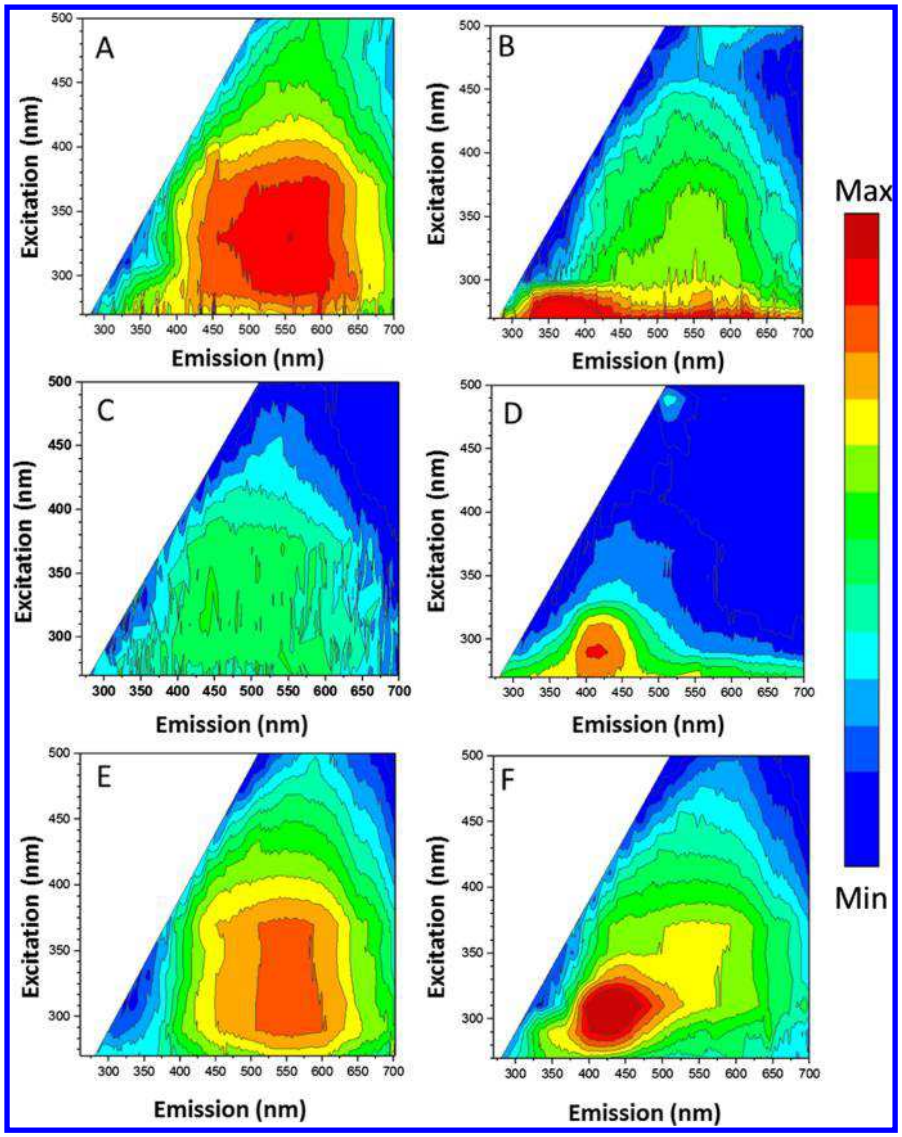

Figure 6. Photoluminescence maps for Graphenea GO dispersions sonicated with 0.6 MJ/g at pH 2 (A) appears to follow the trend found in Figure 5, whereas a repeat measurement (B) shows the possible appearance of OxD, even at a low pH and sonication energy. For a GO sample sonicated with 0.6 MJ/g at pH 10, most measurements do not show the OxD peak (C), but it does appear occasionally (D). A similar case arises for 4 MJ/g at pH 4.5 (E), where the OxD band was sometimes visible in the repeat measurement (F). The intensity in all plots is shown on a logarithmic scale.

As various cell lines respond differently to external stimulants, it was not expected that the A549 cell line demonstrates the same toxicity profile as NIH 3T3. This was indeed the case as GO appeared to be much less toxic on the A549 cell line, demonstrating obvious signs of toxicity only at concentrations over 50 μg/mL. This result is also in agreement with the findings of Hu et al.[46] Interestingly, increased incubation time did not result in lower cell viability. The absence of exposure time dependence has previously been reported for the A549 cell line in other works.[49] We observed little viability difference between the corresponding samples exposed for 24 and 48 h. However, samples exposed to GO for 96 h showed higher viability, especially for the largest flakes. The increased viability is likely because of the cells using GO flakes as a growth surface, with the larger flakes providing a larger growing surface area. A similar observation has been reported in the work of Ruiz et al.[63]

CONCLUSIONS

This work demonstrates probe sonication to be an easy, fast, and reliable method for tailoring the size of GO flakes in aqueous dispersions as needed. It also shows that DLS can be used for rapid and accurate determination of the average GO flake size. Even though DLS provides the equivalent hydrodynamic diameter as the size descriptor, the corresponding surface area of the flakes, whenever required, can be determined by comparison of the DLS results with the AFM size distributions measured for selected flake sizes. The combination of sonication and DLS size assessment facilitates quick and accurate GO flake size modification. Although the lateral dimensions of GO flakes are modified by sonication, their monolayer morphology remains unchanged. At high sonication energies and high alkalinity, OxD is found to detach from the GO framework leading to appearance of a strong distinctive luminescence band at $\lambda_{ex} \approx 290$ nm and $\lambda_{em} \approx 350-450$ nm. The band gap luminescence intensity decreases with increasing pH of dispersions, with a large drop above pH 4.5, which

DOI: 10.1021/acsami.7b08585
ACS Appl. Mater. Interfaces 2017, 9, 28911−28921

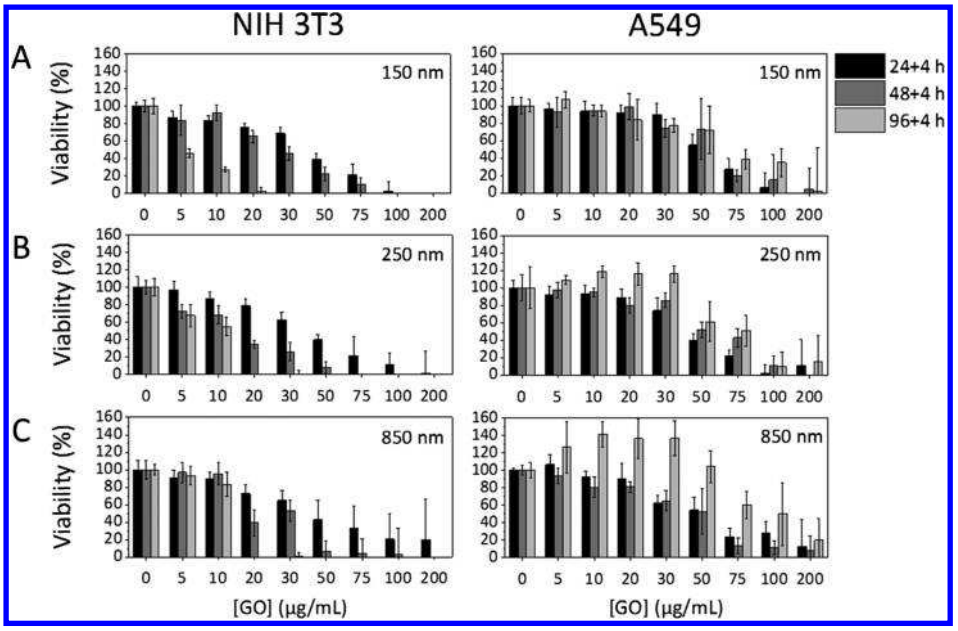

Figure 7. Viability of NIH 3T3 and A549 cells after incubation for 24, 48, and 96 h, with GO flakes of the average size equal to (A) ~150, (B) ~250, and (C) ~850 nm. The WST-8 assay was used.

coincides with the deprotonation of carboxylic acid groups found on the GO framework. Some evidence of photoluminescence intensity variation with the flake size was observed, but the results are mostly inconclusive. Last, cytotoxicity studies show a flake size effect as both cell lines (NIH 3T3 and A549) exposed to small GO flakes have lower viability compared to those exposed to large flakes. Increasing incubation time or GO concentration both result in lower viability of the fibroblast NIH 3T3 cells. The overall viability of the GO-treated A549 cells is much higher compared to the viability of the NIH 3T3 cells, indicating that the toxicity of GO is cell line-dependent.

■ ASSOCIATED CONTENT

Supporting Information

The Supporting Information is available free of charge on the ACS Publications website at DOI: 10.1021/acsami.7b08585.

Additional data on sonication energy and size dependence, AFM images, and GO dispersion stability tests (PDF)

■ AUTHOR INFORMATION

Corresponding Author

*E-mail: shan.zou@nrc-cnrc.gc.ca. Phone: +1-613-949-9675.

ORCID

Shan Zou: 0000-0002-2480-6821

Author Contributions

The manuscript was written through contributions of all authors. All authors have given approval to the final version of the manuscript.

Notes

The authors declare no competing financial interest.

■ ACKNOWLEDGMENTS

The authors wish to thank the National Research Council Canada (NRC) for the facility and financial support. The authors also thank the Natural Sciences and Engineering Research Council of Canada (NSERC) for a Discovery Grant to S.Z.

■ REFERENCES

(1) Si, Y.; Samulski, E. T. Synthesis of Water Soluble Graphene. *Nano Lett.* **2008**, *8*, 1679−1682.

(2) Pei, S.; Cheng, H.-M. The Reduction of Graphene Oxide. *Carbon* **2012**, *50*, 3210−3228.

(3) Mohandoss, M.; Gupta, S. S.; Nelleri, A.; Pradeep, T.; Maliyekkal, S. M. Solar Mediated Reduction of Graphene Oxide. *RSC Adv.* **2017**, *7*, 957−963.

(4) Hou, D.; Liu, Q.; Cheng, H.; Zhang, H.; Wang, S. Green Reduction of Graphene Oxide via Lycium Barbarum Extract. *J. Solid State Chem.* **2017**, *246*, 351−356.

(5) Yang, X.; Zhang, X.; Ma, Y.; Huang, Y.; Wang, Y.; Chen, Y. Superparamagnetic Graphene Oxide−Fe_3O_4 Nanoparticles Hybrid for Controlled Targeted Drug Carriers. *J. Mater. Chem.* **2009**, *19*, 2710−2714.

(6) Wang, Z.; Zhou, X.; Zhang, J.; Boey, F.; Zhang, H. Direct Electrochemical Reduction of Single-Layer Graphene Oxide and Subsequent Functionalization with Glucose Oxidase. *J. Phys. Chem. C* **2009**, *113*, 14071−14075.

(7) Eda, G.; Lin, Y.-Y.; Mattevi, C.; Yamaguchi, H.; Chen, H.-A.; Chen, I.-S.; Chen, C.-W.; Chhowalla, M. Blue Photoluminescence from Chemically Derived Graphene Oxide. *Adv. Mater.* **2010**, *22*, 505−509.

(8) Luo, Z.; Vora, P. M.; Mele, E. J.; Johnson, A. T. C.; Kikkawa, J. M. Photoluminescence and Band Gap Modulation in Graphene Oxide. *Appl. Phys. Lett.* **2009**, *94*, 111909.

(9) Zhou, M.; Wang, Y.; Zhai, Y.; Zhai, J.; Ren, W.; Wang, F.; Dong, S. Controlled Synthesis of Large-Area and Patterned Electrochemically Reduced Graphene Oxide Films. *Chem.—Eur. J.* **2009**, *15*, 6116−6120.

(10) Dikin, D. A.; Stankovich, S.; Zimney, E. J.; Piner, R. D.; Dommett, G. H. B.; Evmenenko, G.; Nguyen, S. T.; Ruoff, R. S. Preparation and Characterization of Graphene Oxide Paper. *Nature* **2007**, *448*, 457−460.

(11) Loh, K. P.; Bao, Q.; Eda, G.; Chhowalla, M. Graphene Oxide as a Chemically Tunable Platform for Optical Application. *Nat. Chem.* **2010**, *2*, 1015−1024.

(12) Hazra, S. K.; Basu, S. Graphene-Oxide Nano Composites for Chemical Sensor Applications. *C* **2016**, *2*, 12.

DOI: 10.1021/acsami.7b08585
ACS Appl. Mater. Interfaces 2017, 9, 28911−28921

(13) Taylor, A. P.; Velásquez-García, L. F. Electrospray-Printed Nanostructured Graphene Oxide Gas Sensors. *Nanotechnology* **2015**, *26*, 505301.
(14) Borini, S.; White, R.; Wei, D.; Astley, M.; Haque, S.; Spigone, E.; Harris, N.; Kivioja, J.; Ryhänen, T. Ultrafast Graphene Oxide Humidity Sensors. *ACS Nano* **2013**, *7*, 11166−11173.
(15) Wang, Y.; Shi, Z.; Huang, Y.; Ma, Y.; Wang, C.; Chen, M.; Chen, Y. Supercapacitor Devices Based on Graphene Materials. *J. Phys. Chem. C* **2009**, *113*, 13103−13107.
(16) Zhang, L. L.; Zhao, S.; Tian, X. N.; Zhao, X. S. Layered Graphene Oxide Nanostructures with Sandwiched Conducting Polymers as Supercapacitor Electrodes. *Langmuir* **2010**, *26*, 17624−17628.
(17) Liu, J.; Cui, L.; Losic, D. Graphene and Graphene Oxide as New Nanocarriers for Drug Delivery Applications. *Acta Biomater.* **2013**, *9*, 9243−9257.
(18) Zhang, L.; Xia, J.; Zhao, Q.; Liu, L.; Zhang, Z. Functional Graphene Oxide as a Nanocarrier for Controlled Loading and Targeted Delivery of Mixed Anticancer Drugs. *Small* **2010**, *6*, 537−544.
(19) Sun, X.; Liu, Z.; Welsher, K.; Robinson, J. T.; Goodwin, A.; Zaric, S.; Dai, H. Nano-Graphene Oxide for Cellular Imaging and Drug Delivery. *Nano Res.* **2008**, *1*, 203−212.
(20) Yousefi, N.; Gudarzi, M. M.; Zheng, Q.; Aboutalebi, S. H.; Sharif, F.; Kim, J.-K. Self-Alignment and High Electrical Conductivity of Ultralarge Graphene Oxide−Polyurethane Nanocomposites. *J. Mater. Chem.* **2012**, *22*, 12709−12717.
(21) Li, C.; Shi, G. Three-Dimensional Graphene Architectures. *Nanoscale* **2012**, *4*, 5549−5563.
(22) Su, C.-Y.; Xu, Y.; Zhang, W.; Zhao, J.; Tang, X.; Tsai, C.-H.; Li, L.-J. Electrical and Spectroscopic Characterizations of Ultra-Large Reduced Graphene Oxide Monolayers. *Chem. Mater.* **2009**, *21*, 5674−5680.
(23) Xu, P.; Xu, T.; Yu, H. Graphene-Oxide (GO) Nano-Sheets: Lateral and Vertical Size-Effects on Chemical-Gas Sensitivity Enhancement. In *2016 IEEE 29th International Conference on Micro Electro Mechanical Systems (MEMS)*: Shanghai, China, 2016.
(24) Liu, Z.; Robinson, J. T.; Sun, X.; Dai, H. PEGylated Nanographene Oxide for Delivery of Water-Insoluble Cancer Drugs. *J. Am. Chem. Soc.* **2008**, *130*, 10876−10877.
(25) Shin, K.-Y.; Lee, S.; Hong, S.; Jang, J. Graphene Size Control via a Mechanochemical Method and Electroresponsive Properties. *ACS Appl. Mater. Interfaces* **2014**, *6*, 5531−5537.
(26) Sun, X.; Luo, D.; Liu, J.; Evans, D. G. Monodisperse Chemically Modified Graphene Obtained by Density Gradient Ultracentrifugal Rate Separation. *ACS Nano* **2010**, *4*, 3381−3389.
(27) Luo, J.; Cote, L. J.; Tung, V. C.; Tan, A. T. L.; Goins, P. E.; Wu, J.; Huang, J. Graphene Oxide Nanocolloids. *J. Am. Chem. Soc.* **2010**, *132*, 17667−17669.
(28) Wang, X.; Bai, H.; Shi, G. Size Fractionation of Graphene oxide Sheets by pH-Assisted Selective Sedimentation. *J. Am. Chem. Soc.* **2011**, *133*, 6338−6342.
(29) Zhang, H.; Peng, C.; Yang, J.; Lv, M.; Liu, R.; He, D.; Fan, C.; Huang, Q. Uniform Ultrasmall Graphene Oxide Nanosheets with Low Cytotoxicity and High Cellular Uptake. *ACS Appl. Mater. Interfaces* **2013**, *5*, 1761−1767.
(30) Chen, H.; Müller, M. B.; Gilmore, K. J.; Wallace, G. G.; Li, D. Mechanically Strong, Electrically Conductive, and Biocompatible Graphene Paper. *Adv. Mater.* **2008**, *20*, 3557−3561.
(31) Tian, Y.; Cao, Y.; Wang, Y.; Yang, W.; Feng, J. Realizing Ultrahigh Modulus and High Strength of Macroscopic Graphene Oxide Papers Through Crosslinking of Mussel-Inspired Polymers. *Adv. Mater.* **2013**, *25*, 2980−2983.
(32) Putz, K. W.; Compton, O. C.; Palmeri, M. J.; Nguyen, S. T.; Brinson, L. C. High-Nanofiller-Content Graphene Oxide-Polymer Nanocomposites via Vacuum-Assisted Self-Assembly. *Adv. Funct. Mater.* **2010**, *20*, 3322−3329.
(33) Hu, K.; Kulkarni, D. D.; Choi, I.; Tsukruk, V. V. Graphene-Polymer Nanocomposites for Structural and Functional Applications. *Prog. Polym. Sci.* **2014**, *39*, 1934−1972.
(34) Qi, X.; Zhou, T.; Deng, S.; Zong, G.; Yao, X.; Fu, Q. Size-Specified Graphene Oxide Sheets: Ultrasonication Assisted Preparation and Characterization. *J. Mater. Sci.* **2014**, *49*, 1785−1793.
(35) Luo, Z.-J.; Geng, H.-Z.; Zhang, X.; Du, B.; Ding, E.-X.; Wang, J.; Lu, Z.; Sun, B.; Wang, J.; Liu, J. A TimeSaving, Low-Cost, High-Yield Method for the Synthesis of Ultrasmall Uniform Graphene Oxide Nanosheets and their Application in Surfactants. *Nanotechnology* **2015**, *27*, 055601.
(36) Ye, S.; Feng, J. The Effect of Sonication Treatment of Graphene Oxide on the Mechanical Properties of the Assembled Films. *RSC Adv.* **2016**, *6*, 39681−39687.
(37) Cai, C.; Sang, N.; Shen, Z.; Zhao, X. Facile and Size-Controllable Preparation of Graphene Oxide Nanosheets using High Shear Method and Ultrasonic Method. *J. Exp. Nanosci.* **2017**, DOI: 10.1080/17458080.2017.1303853.
(38) Mkhoyan, K. A.; Contryman, A. W.; Silcox, J.; Stewart, D. A.; Eda, G.; Mattevi, C.; Miller, S.; Chhowalla, M. Atomic and Electronic Structure of Graphene-Oxide. *Nano Lett.* **2009**, *9*, 1058−1063.
(39) Park, S.; Ruoff, R. S. Chemical Methods for the Production of Graphenes. *Nat. Nanotechnol.* **2009**, *4*, 217−224.
(40) Dutta, P.; Nandi, D.; Datta, S.; Chakraborty, S.; Das, N.; Chatterjee, S.; Ghosh, U. C.; Halder, A. Excitation Wavelength Dependent UV Fluorescence of Dispersed Modified Graphene Oxide: Effect of pH. *J. Lumin.* **2015**, *168*, 269−275.
(41) Galande, C.; Mohite, A. D.; Naumov, A. V.; Gao, W.; Ci, L.; Ajayan, A.; Gao, H.; Srivastava, A.; Weisman, R. B.; Ajayan, P. M. Quasi-Molecular Fluorescence from Graphene Oxide. *Sci. Rep.* **2011**, *1*, 85.
(42) Oberdörster, G.; Oberdörster, E.; Oberdörster, J. Nanotoxicology: An Emerging Discipline Evolving from Studies of Ultrafine Particles. *Environ. Health Perspect.* **2005**, *113*, 823−839.
(43) Aillon, K. L.; Xie, Y.; El-Gendy, N.; Berkland, C. J.; Forrest, M. L. Effects of Nanomaterial Physicochemical Properties on in vivo Toxicity. *Adv. Drug Delivery Rev.* **2009**, *61*, 457−466.
(44) Xia, T.; Li, N.; Nel, A. E. Potential Health Impact of Nanoparticles. *Annu. Rev. Public Health* **2009**, *30*, 137−150.
(45) Liao, K.-H.; Lin, Y.-S.; Macosko, C. W.; Haynes, C. L. Cytotoxicity of Graphene Oxide and Graphene in Human Erythrocytes and Skin Fibroblasts. *ACS Appl. Mater. Interfaces* **2011**, *3*, 2607−2615.
(46) Hu, W.; Peng, C.; Lv, M.; Li, X.; Zhang, Y.; Chen, N.; Fan, C.; Huang, Q. Protein Corona-Mediated Mitigation of Cytotoxicity of Graphene Oxide. *ACS Nano* **2011**, *5*, 3693−3700.
(47) Zhang, X.; Hu, W.; Li, J.; Tao, L.; Wei, Y. A comparative study of cellular uptake and cytotoxicity of multi-walled carbon nanotubes, graphene oxide, and nanodiamond. *Toxicol. Res.* **2012**, *1*, 62−68.
(48) Lu, C.-H.; Yang, H.-H.; Zhu, C.-L.; Chen, X.; Chen, G.-N. A Graphene Platform for Sensing Biomolecules. *Angew. Chem., Int. Ed.* **2009**, *48*, 4785−4787.
(49) Chang, Y.; Yang, S.-T.; Liu, J.-H.; Dong, E.; Wang, Y.; Cao, A.; Liu, Y.; Wang, H. In Vitro Toxicity Evaluation of Graphene Oxide on A549 Cells. *Toxicol. Lett.* **2011**, *200*, 201−210.
(50) Wang, K.; Ruan, J.; Song, H.; Zhang, J.; Wo, Y.; Guo, S.; Cui, D. Biocompatibility of Graphene Oxide. *Nanoscale Res. Lett.* **2011**, *6*, 8.
(51) Das, S.; Singh, S.; Singh, V.; Joung, D.; Dowding, J. M.; Reid, D.; Anderson, J.; Zhai, L.; Khondaker, S. I.; Self, W. T.; Seal, S. Oxygenated Functional Group Density on Graphene Oxide: Its Effect on Cell Toxicity. *Part. Part. Syst. Charact.* **2013**, *30*, 148−157.
(52) LS Instruments. *Dynamic Light Scattering: Measuring the Particle Size Distribution*. http://www.lsinstruments.ch/technology/dynamic_light_scattering_dls/ (accessed Apr 6, 2017).
(53) Gonçalves, G.; Vila, M.; Bdikin, I.; de Andrés, A.; Emami, N.; Ferreira, R. A. S.; Carlos, L. D.; Grácio, J.; Marques, P. A. A. P. Breakdown into Nanoscale of Graphene Oxide: Confined Hot Spot Atomic Reduction and Fragmentation. *Sci. Rep.* **2014**, *4*, 6735.

(54) Daly, M.; Cao, C.; Sun, H.; Sun, Y.; Filleter, T.; Singh, C. V. Interfacial Shear Strength of Multilayer Graphene Oxide Films. *ACS Nano* **2016**, *10*, 1939−1947.
(55) Compton, O. C.; An, Z.; Putz, K. W.; Hong, B. J.; Hauser, B. G.; Brinson, L. C.; Nguyen, S. T. Additive-Free Hydrogelation of Graphene Oxide by Ultrasonication. *Carbon* **2012**, *50*, 3399−3406.
(56) Lotya, M.; Rakovich, A.; Donegan, J. F.; Coleman, J. N. Measuring the Lateral Size of Liquid-Exfoliated Nanosheets with Dynamic Light Scattering. *Nanotechnology* **2013**, *24*, 265703.
(57) Lee, C.; Wei, X.; Kysar, J. W.; Hone, J. Measurement of the Elastic Properties and Intrinsic Strength of Monolayer Graphene. *Science* **2008**, *321*, 385−388.
(58) Shang, J.; Ma, L.; Li, J.; Ai, W.; Yu, T.; Gurzadyan, G. G. The Origin of Fluorescence from Graphene Oxide. *Sci. Rep.* **2012**, *2*, 792.
(59) Kochmann, S.; Hirsch, T.; Wolfbeis, O. S. The pH Dependence of the Total Fluorescence of Graphite Oxide. *J. Fluoresc.* **2012**, *22*, 849−855.
(60) Thomas, H. R.; Day, S. P.; Woodruff, W. E.; Vallés, C.; Young, R. J.; Kinloch, I. A.; Morley, G. W.; Hanna, J. V.; Wilson, N. R.; Rourke, J. P. Deoxygenation of Graphene Oxide: Reduction or Cleaning? *Chem. Mater.* **2013**, *25*, 3580−3588.
(61) Rourke, J. P.; Pandey, P. A.; Moore, J. J.; Bates, M.; Kinloch, I. A.; Young, R. J.; Wilson, N. R. The Real Graphene Oxide Revealed: Stripping the Oxidative Debris from the Graphene-Like Sheets. *Angew. Chem., Int. Ed.* **2011**, *50*, 3173−3177.
(62) Thomas, H. R.; Vallés, C.; Young, R. J.; Kinloch, I. A.; Wilson, N. R.; Rourke, J. P. Identifying the Fluorescence of Graphene Oxide. *J. Mater. Chem. C* **2013**, *1*, 338−342.
(63) Ruiz, O. N.; Fernando, K. A. S.; Wang, B.; Brown, N. A.; Luo, P. G.; McNamara, N. D.; Vangsness, M.; Sun, Y.-P.; Bunker, C. E. Graphene Oxide: A Nonspecific Enhancer of Cellular Growth. *ACS Nano* **2011**, *5*, 8100−8107.

DOI: 10.1021/acsami.7b08585
ACS Appl. Mater. Interfaces 2017, 9, 28911−28921